Draft version April 1, 2017
Typeset using LaTeX **twocolumn** style in AASTeX61

OPTIFCAL OBSERVATIONS OF AN EXTRAORDINARILY YOUNG TYPE IA SUPERNOVA IPTF16ABC

Yi Cao[1] and Friends[2]

[1] *eScience Institute and Astronomy Department, University of Washington, Seattle, WA 98195*
[2] *the intermediate Palomar Transient Factory*

(Received April 1, 2017; Revised; Accepted)

Submitted to ApJ

ABSTRACT

We report discovery of an extraordinarily young Type Ia supernova iPTF16abc by the intermediate Palomar Transient Factory. Our first observation was made only 0.18 days after the onset of the supernova explosion. Our analysis shows that the early emission of this supernova dominantly comes from the radioactive decay instead of supernova shock breakout or collision between the ejecta and a possible companion star. The fast initial rise of the supernova, the velocity evolution of spectral lines, and the strong and short-lived carbon feature in the earliest spectra together provide strong evidence of strong mixing of synthesized radioactive elements during the supernova explosion.

Keywords: methods: observational — supernovae: individual (iPTF16abc)

Corresponding author: Yi Cao
ycao16@uw.edu

1. INTRODUCTION

Although Type Ia supernovae (SNe Ia) have been extensively used as standardizable candles, their progenitor systems and explosion mechanisms remain unclear (see a recent review by Maoz et al. 2014). Observations of extremely young events are one promising avenue to further constrain this problem.

While the shock breakout of a SN Ia occurs on a minisecond timescale, the subsequent cooling of the unbinded ejecta during its adiabatic expansion produces thermal emission until the radioactive energy heats up the photosphere of the ejecta. The thermal emission during this adiabatic expansion phase therefore be used to infer the original size of the exploding star (Piro et al. 2010; Rabinak & Waxman 2011). For example, the earliest observations of SN2011fe allowed Bloom et al. (2012) to conclude that the radius of the progenitor star is $\lesssim 0.01 R_\odot$ where $R_\odot$ is the solar radius and that the progenitor has to be compact and degenerate. However, because of the small surface area of the progenitor star, the cooling emission is not luminous. As a result, this method is only applicable to events within ~ 10 Mpc.

If a SN Ia is born in the single degenerate (SD) channel (Whelan & Iben 1973), then the SN ejecta slams into the companion and produces a non-thermal X-ray flash. Once the fast-moving ejecta covers the collision region, the collision heats up the surrounding material. The collisional energy is then released near the direction of the companion (about a few to ten percent of the 4π solid angle) as thermal emission with a spectrum that peaks in the UV (Kasen 2010). This SN-companion collisional signature serves as a "smoking gun" for the SD channel, because it is not expected in the competing double-degenerate channel ycao: REF. This signature has been searched in several nearby SNe Ia and a few samples of distant SNe Ia (Hayden et al. 2010; Bianco et al. 2011; Foley et al. 2012; Bloom et al. 2012; Olling et al. 2015; Zheng et al. 2013; Goobar et al. 2015; Shappee et al. 2016; Im et al. 2015), only in a low-velocity SNe Ia was a strong and declining ultraviolet (UV) pulse seen within a few days of the explosion.

More commonly, the observed light curve of a SN Ia is purely powered by the radioactive decay of synthesized ^{56}Ni. Depending on the depth of the shallowest layer where ^{56}Ni is deposited, the SN may experience a dark period before the radioactive energy diffuses to the photosphere. According to the calculation in Piro & Morozova (2016), strong mixing leads to a short dark period and a fast initial rise, while weak mixing results in a long dark period and a moderate initial rise. Measuring the initial rise rate of a SN Ia allows us to constrain the mixing level of the SN ejecta which is closely related to the explosion mechanism.

In this paper, we report observations of a young SN Ia iPTF16abc within a day of its explosion. This SN was discovered by the intermediate Palomar Transient Factory on 2016 April 3.36[1] at R.A. = $13^h34^m45.49^s$, Dec. = $+13^d51^m14.3^s$ (J2000) with a g-band magnitude of 21.31 ± 0.27 (Cao et al. 2016; Miller et al. 2016). The transient is spatially coincident with a tidal tail of the galaxy NGC 5221 at 100 Mpc. No activity was detected at the same location down to $g = 22.1$ mag on April 2.42. Our spectroscopic follow-up compaign classified iPTF16abc as a normal SN Ia (Cenko et al. 2016).

This paper is organized as follows: Section 2 describes photometric and spectroscopic observations of iPTF16abc. Section 3 establishes that iPTF16abc is a normal SN Ia in NGC 5221. Section 4 analyzes the early light curve and spectra.

2. OBSERVATIONS

As part of the iPTF transient survey in the 2016 spring quarter, the field of iPTF16abc was observed in g- or R-band every night by the CFH12K camera (Starr et al. 2000) on the 48-inch telescope at Palomar Observatory (P48). The images were processed by the IPAC image subtraction and discovery pipeline which subtracts off the background galaxy light with stacked pre-SN images and performs forced point-spread-function (PSF) photometry at the location of the SN. The photometry is then calibrated to the PTF photometric catalog (Ofek et al. 2012).

After discovery, we utilized the rainbow camera of the SED Machine (ycao: REF) mounted on the 60-inch telescope at Palomar Observatory (P60) to undertake photometric observations in g, r and i filters. The image differencing against the archival SDSS images and forced PSF photometry on the subtracted images were performed by the Fremling Automated Pipeline (Fremling et al. 2016). The photometry is also calibrated to the SDSS catalog ycao: which DR?.

Las Cambres Observatory Global Network (LCOGT) also carry out photometric observations in the $BVgri$ filters with its 1-m telescope network. PSF photometry was measured on these images using the `lcogtsnpipe` pipeline (Valenti et al. 2016). The BV magnitudes are calibrated to the Fourth USNO CCD Astrograph Catalog (Zacharias et al. 2013), and the gri magnitudes are calibrated to SDSS Data Release 6 (Adelman-McCarthy et al. 2008).

[1] all times in this paper are in UTC.

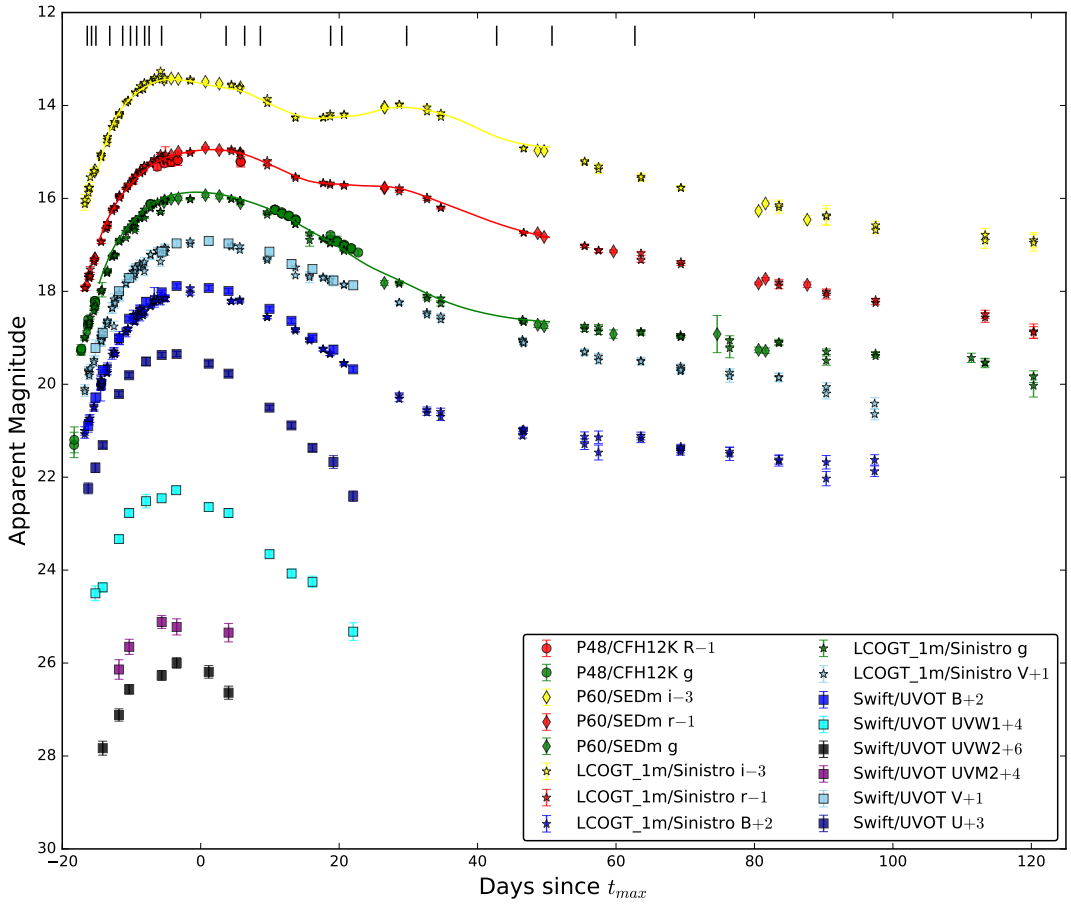

Figure 1. Multi-band light curves of iPTF16abc are shown. Filters are denoted by different colors and observation instruments by different markers. The t_{max} time is the B-band maximum determined by SALT2 (Section 3.2). The solid curves are best-fit results from SALT2. The black ticks near the top of the figure shows epochs of spectroscopic observations.

In space, *Swift* observed iPTF16abc for 14 epochs, covering from the very early phase to the post-peak phase. Aperture photometry are carried out on the images taken by its Ultraviolet-Optical Telescope (UVOT) with the usual procedures in the HEASoft and corrected for the coincident loss and aperture loss. The image counts are converted to physical fluxes using the latest calibration (Breeveld et al. 2011). No pre-SN UVOT image at the SN location is available in the *Swift* archive. Visual inspection to the UVOT images suggests that the background galaxy light in the UVOT filters is probably negligible. No X-ray emission was detected at the location of the SN by the X-ray Telescope (XRT) in any of these epochs.

The multi-color light curves of iPTF16abc are illustrated in Figure 1. For convenience, magnitudes in *all* filters are in the AB system with a zero point of 3631 Jy.

Spectroscopic observations of iPTF16abc were undertaken with a variety of telescopes and instruments in multiple epochs spanning from a couple of days after explosion to two months after its maximum. An observing log is listed in Table 1. Data reduction is undertaken with usual routines in IDL/Python. Except for the high-resolution spectra obtained by VLT instruments, the optical spectral evolution of iPTF16abc is illustrated in Figure 2.

3. REDDENING, CLASSIFICATION AND HOST GALAXY

3.1. *Reddening*

Table 1. Spectroscopic observations of iPTF16abc

Observation MJD	SN phase	Telescope	Instrument	Wavelength Coverage (Å)
57483.26	−16.4	DCT	DeVeny[1]	3301–7499
57483.88	−15.8	Gemini-North	GMOS[2]	3800–9200
57484.51	−15.1	Keck-II	DEIMOS[3]	5500–8099
57486.51	−13.1	Keck-II	DEIMOS[3]	5500–8099
57488.38	−11.3	Keck-I	LRIS[4]	3055–10411
57489.51	−10.1	LCOGT-2m	FLOYDS[5]	3301–8999
57490.40	−9.3	LCOGT-2m	FLOYDS[5]	3301–9999
57491.55	−8.1	LCOGT-2m	FLOYDS[5]	3300–9998
57492.20	−7.5	VLT	X-shooter[6]	3300–24550
57494.00	−5.7	VLT	UVES[7]	
57503.32	+3.7	LCOGT-2m	FLOYDS[5]	3300–9999
57506.00	+6.3	NOT	ALFOSC[8]	3602–8098
57508.27	+8.6	LCOGT-2m	FLOYDS[5]	3301–9999
57518.42	+18.8	Keck-I	LRIS[4]	3071–10208
57520.03	+20.4	VLT	X-shooter[6]	3300–24789
57529.40	+29.8	LCOGT-2m	FLOYDS[5]	4000–8998
57542.41	+42.8	LCOGT-2m	FLOYDS[5]	4000–8998
57550.40	+50.8	LCOGT-2m	FLOYDS[5]	4001–8999
57562.38	+62.7	LCOGT-2m	FLOYDS[5]	4800–9300

[1] The Deveny Spectrograph (Bida et al. 2014)

[2] The Gemini Multi-Object Sectrograph (Hook et al. 2004)

[3] DEep Imaging Multi-Object Spectrograph (Faber et al. 2003)

[4] Low-Resolution Imaging Spectrometer (Oke et al. 1995)

[5] FLOYDS https://lco.global/observatory/instruments/floyds

[6] X-shooter (Vernet et al. 2011)

[7] Ultraviolet and Visual Echelle Spectrograph (Dekker et al. 2000)

[8] The Andalucia Faint Object Spectrograph and Camera http://www.not.iac.es/instruments/alfosc

The foreground Galactic extinctioin along the directionof iPTF16abc has $E(B-V) = 0.0279$ mag (Schlafly & Finkbeiner 2011).

In the highest-resolution spectrum of iPTF16abc by UVES, individual components of both Ca II H+K and Na I D doublets show double-absorption profiles (Figure 3), indicating two sources of absorption along the line of sight. Fitting two Gaussian kernels to each line of the Na I doublet simultaneously leads to redshifts of $0.02313820 \pm 0.00000032$ and $0.02322408 \pm 0.00000033$. The total equivalent widths of the Na I D1 and D2 lines are 0.595 ± 0.009 Å and 0.609 ± 0.008 Åm, respectively. Using the empirical relation between the equivalent width of Na I D lines and reddening $E(B-V)$ (Poznanski et al. 2012), we derive $E(B-V) = 0.361 \pm 0.025$mag. We caution that the empirical relation has a quite large scatter.

In the X-shooter spectra of iPTF16abc, we also identify narrow absorption features K I 7665 Åand 7699 Åat consistent redshifts. However, the resolution of the X-shooter spectra is not fine enough to resolve the double-absorption profiles of Ca II and Na I. The X-shooter spectra do not show the diffusive interstellar band at 5780 Åas well. Albeit some debates (e.g., Phillips et al.

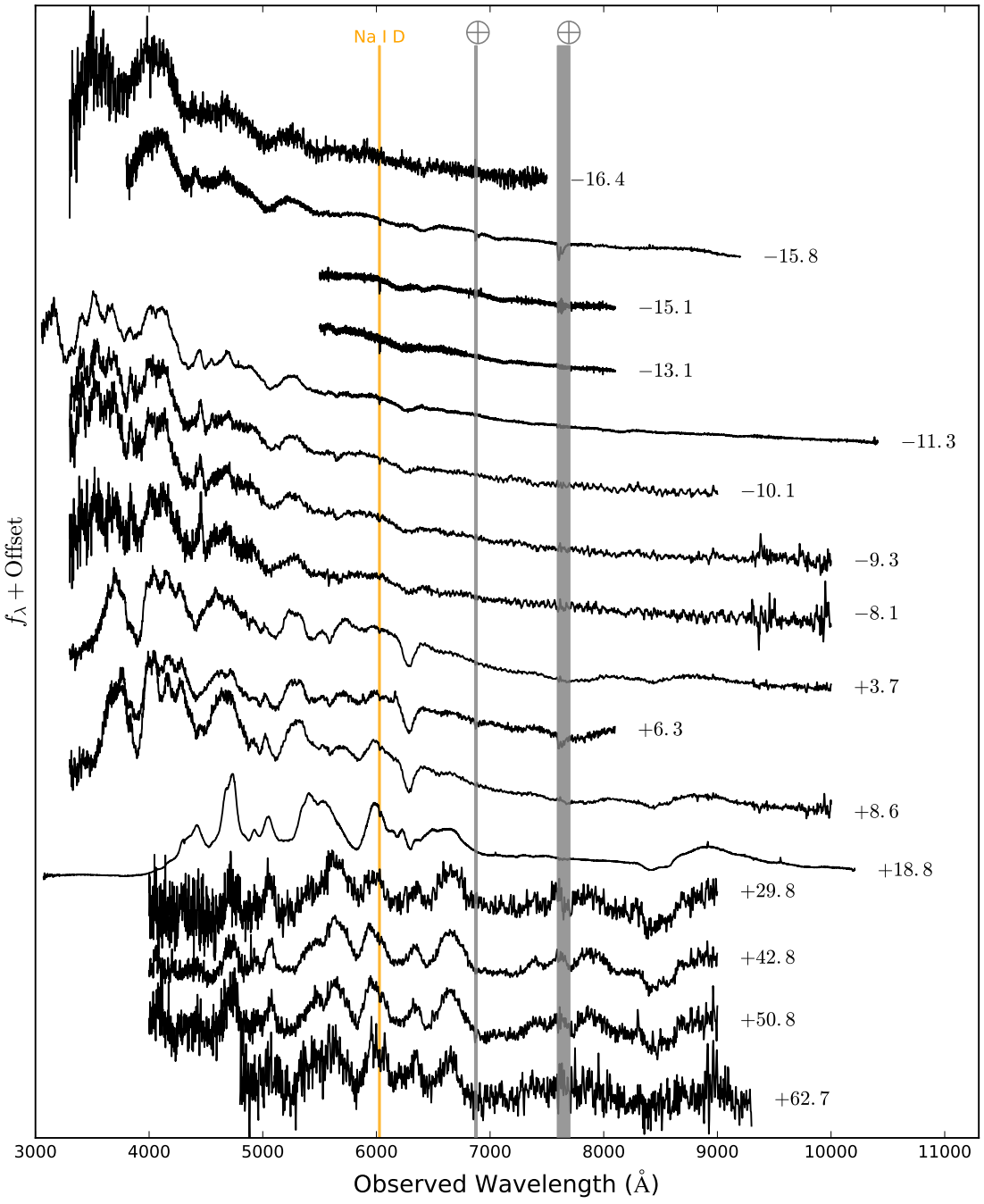

Figure 2. Low-resolution spectra of iPTF16abc are shown in the chronical orders. In order for better illustration, each spectrum is normalized by the median flux value between 6,000 and 7,000 Å and offset properly. The phases in units of days are noted next to corresponding spectra. Telluric absorption bands are grayed out. The narrow Na I D absorption is also highlighted in orange.

2013), the $E(B-V)$ value derived from Na I D absorption provides the best estimate in the case of iPTF16abc.

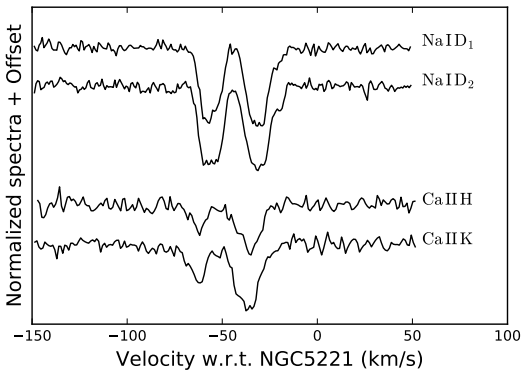

Figure 3. Narrow absorption lines of iPTF16abc are shown in this figure. The zero velocity corresponds to the redshift of the apparent host NGC 5221.

The Na I D doublet are seen in multiple spectra spanning from pre-peak to post-peak phases. Despite the instrumental widening of different instrument configurations, we do not detect obvious variation in the profiles of the doublet.

We also note in Figure 3 that the absorption profiles of Ca II H+K are quite different from those of Na I D doublet, implying that the dust compositions in the two absorption sources may have some difference.

3.2. *Classfication*

We run Supernova Identification (SNID; Blondin & Tonry 2007) on the low-resolution spectrum of iPTF16abc at +18.8 and found best matches to normal SNe Ia. In fact, the characteristic features of a SN Ia, such as Si II, S II, can be easily identified in the spectra of iPTF16abc (Figure 2).

Next we standardize the light curve of iPTF16abc by feeding its P48 and P60 light curves into the `sncosmo` module[2] and fit a light curve model, which composes of the SALT2 template (Guy et al. 2007) modified by the line-of-sight extinction curve (Fitzpatrick 1999) with $E(B-V)$ values from Section 3.1 and $R_V = 3.1$. We obtain the rest-frame B-band peak time $\mathrm{MJD}_{max} = 57499.65 \pm 0.02$, the coefficient of the zeroth principle component $x_0 = 0.0275 \pm 0.0002$, the coefficient of the first principle component $x_1 = 1.200 \pm 0.043$, and the color term $c = -0.3353 \pm 0.0054$. The best-fit model also gives an unreddened apparent peak magnitude of $m_B^* = 14.4$ mag in the SN rest frame.

For convenience, in the following sections, we define the best-fit value $\mathrm{MJD}_{max} = 57499.65$ as phase $t = 0$.

[2] The `sncosmo` Python module is available at https://sncosmo.readthedocs.io/en/v1.4.x/.

3.3. *Host Galaxy*

After establishing iPTF16abc as a normal SN ia, we use the latest calibration (Betoule et al. 2014) of the Phillips relation (Phillips 1993) using m_B^*, x_1 and c to derive a distance modulus $\mu = 34.66 \pm 0.03$ mag to the SN, provided that the host galaxy of iPTF16abc has a stellar mass less than $10^{10} M_\odot$.

The location of iPTF16abc is spatially coincident with a tidal tail of galaxy NGC 5221. Theureau et al. (2007) derived a distance modulus of 35.0 ± 0.4 mag from the Tully-Fisher relation. This distance modulus is consistent with that of iPTF16abc.

Separately, Theureau et al. (1998) observed the 21-cm line in this galaxy and measured a redshift of 0.0233303 ± 0.000027. The two components in the Na I D have a relative velocity of $-57.6 \pm 8.1\,\mathrm{km\,s^{-1}}$ and $-31.8 \pm 8.1\,\mathrm{km\,s^{-1}}$, suggesting that both absorption resources are probaly located on the tidal tail of NGC 5221.

4. FIRST LIGHT AND EXPLOSION TIME

In this section, we estimate the first light and explosion time of iPTF16abc.

4.1. *Light Curve Fit*

Extrapolation of the earliest-phase light curve with a simple mathematical model is usually used to estimate the first light time of a SN. In theory, Arnett (1982) derived a quadratic law for an ideal expanding fireball with a constant temperature. In order to account for variation of photospheric temperatures during expansion, we utilize a power-law curve to model the early light curve.

$$f(t) \begin{cases} = 0, \text{ when } t < t_0 \\ \propto (t - t_0)^\alpha, \text{ when } t > t_0 \end{cases} . \quad (1)$$

Since the first few detections of the SN were made in the g band, our modeling is limited to the early g-band light curve. We minimize χ^2 in a large search grid of t_0, α and the proportionality constant. We also note that the definition of the time window for the early light curve may affect the fitting result, so we experiment the fitting procedure with different time windows. The modeling results show that the SN flux between $t = -19$ days and $t = -15$ days rises approximately linearly. Figure 4 shows the best-fit result and the joint marginal distribution of t_0 and α. With the best-fit model of

$\alpha = 0.92$ and $t_0 = -18.47$ days, our first observation was made only 0.18 day after the first light of the SN. The total rise time to the B-band peak is 18.47 days.

Starting from $t = -15$ days, the g-band light curve rises significantly faster than the best-fit model above, indicating a greater value of the power-law index α. In fact, the light curve between $t = -14$ and $t = -8$ days can be fitted with another power law of index 1.40. In another word, the whole light curve before $t = -8$ days can be approximated by a broken power-law model (e.g., Zheng et al. 2013, 2014; Zheng & Filippenko 2016; Zheng et al. 2016).

As discussed in Section 4.4, the initial light curve of iPTF16abc is probably purely powered by radioactive decay of ^{56}Ni. Therefore, the initial rise of the light curve depends on the depth of the shallowest layer where ^{56}Ni is deposited (Piro & Nakar 2014). According to theoretical mdels (Piro & Morozova 2016), the linearly rising light curve implies strong mixing of ^{56}Ni in the ejecta. As a result, the time lag between the SN explosion and the initial rise of the radioactively powered light curve is negligible.

4.2. *Expansion Velocity Fit*

In order to constrain the explosion time of the SN independently of the SN light curve, Piro & Nakar (2014) suggested to measure the expansion velocities of the photosphere, because the expansion of the ejecta starts at the onset of the SN explosion. Assuming a constant opacity in the ejecta, the photospheric velocity evolves as $v_{ph} \propto (t - t_{exp})^{-0.22}$. While the photospheric velocities are not easy to measure, line velocities of Si II or Ca II are usually used to approximate the photospheric velocities (Piro & Nakar 2014; Shappee et al. 2016).

In the case of iPTF16abc, the Ca II IR triplet is very weak in the spectra probably due to high temperatures in the ejecta. Thus we perform our measurements on the Si II 6355 line. Visual inspection of the spectra shows no sign of multi-velocity components of Si II, and that the C II 6580 line overlaps the red wing of the Si II line. Consequently we apply a mathematical model of two gaussian kernels superposed on a linear term, which accounts for the absorption of Si II and C II and the continuum component, respectively, to approach the observed spectra between 5,900 and 6,500 Å(rest-frame). The expansion velocity of Si II is calculated at the central wavelength of the Si II Gaussian kernel.

We fit the measured velocities of Si II 6355 line to the $v \propto (t - t_{exp})^{-0.22}$ model by minimizing the χ^2 value and find the best-fit explosion time $t_{exp} = -17.95$ days with a 3-σ confidence interval between -17.4 days and -18.3 days (Figure 5). We also alter the power-law index to -0.20 and -0.24 to examine how sensitively the result depends on the assumed power-law index. we find consistent results within respective 3-σ confidence intervals.

Keeping in mind that t_{exp} has a very large uncertainty mostly due to the assumption in the $v \propto (t - t_{exp})^{-0.22}$ model, we compare the estimated t_{exp} to t_0 (left panel of Figure 5) and find that $t_0 \lessapprox t_{exp}$. Since physical causality requires $t_{exp} < t_0$, we draw a qualitative conclusion that $t_0 \simeq t_{exp}$. This conclusion is consistent with our inference from the early light curve analysis in Section 4.1.

With t_{exp}, we estimate the actual rise time of iPTF16abc from the SN explosion to its B-band maximum to be 17.95 days. In comparison, SN2011fe has $t_0 = -17.7$ days (Pereira et al. 2013) with a preceding dark period of ~ 1 day (Piro & Nakar 2014). ASASSN-14lp has $t_0 = -16.94$ days with a preceding dark period of about acouple of days (Shappee et al. 2016). This comparison suggests that the actual rise time of a SN Ia between the SN explosion and the B-band maximum is roughly a constant, which largely depends on the total mass of synthesized ^{56}Ni.

4.3. *Strong and Short-Lived Carbon Features*

Another intriguing spectral feature of iPTF16abc is strong absorption of C II 6580 and C II 7234 lines. Our analysis on the Si II 6355 line also allows us to measure the velocities and pseudo-equivalent widths (pEWs) of C II 6580. We also fit a Gaussian kernel superposing on a linear term to the spectral region near the C II 7234 line to measure its velocity and pseudo-equivalent width. The velocity evolution of C II is shown in the right panel of Figure 5 and the pEW evolution in Figure 6.

Our measurements show that the strong C II absorption only appears in the very early phases. In the spectrum taken at $t = -15.8$ days, the pEW of C II 6580 is comparable to that of Si II 6355. Then the pEW of C II decreases until they disappear at about $t = -10$ days.

Formation of C II absorption requires existence of both unburned carbon and ^{56}Ni, the latter of which is responsible to ionize the carbon atoms. The strong and short-lived C II features observed in the spectra of iPTF16abc show that a certain amount of carbon atoms exist in the outer layers of the ejecta and that ^{56}Ni atoms are also strongly mixed in the same layers. This provides a third piece of evidence to strong mixing in the iPTF16abc ejecta.

Carbon signatures are seen in over 1/4 of all normal SNe Ia before maxima (Parrent et al. 2011; Silverman & Filippenko 2012; Thomas et al. 2011), but the signatures are usually weak. Even in SN2011fe, the

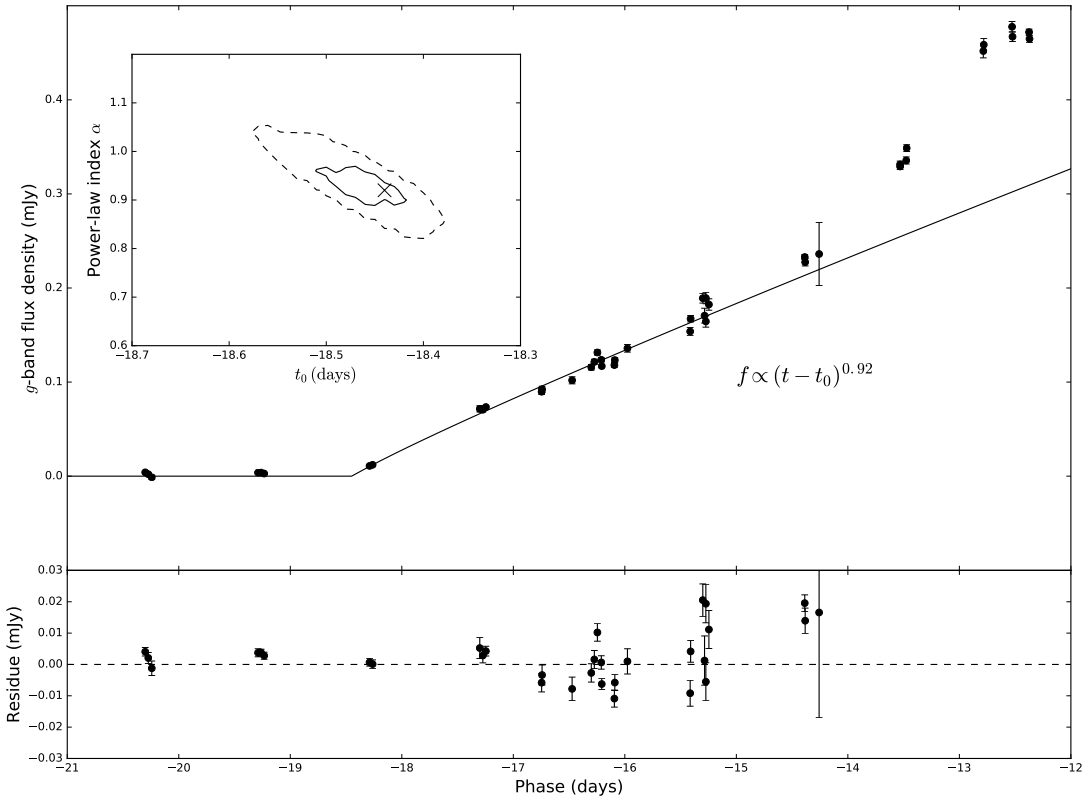

Figure 4. Broken Power low fitting to the early g-band light curve. The best-fit model of $\alpha = 0.92$ and $t_0 = -18.47$ days and corresponding residues are shown in the top and bottom panels, respectively. The joint distribution of t_0 and α is illustrated in the inset of the upper panel. The solid and dashed contours represent the 68% and 99.7% confidence levels.

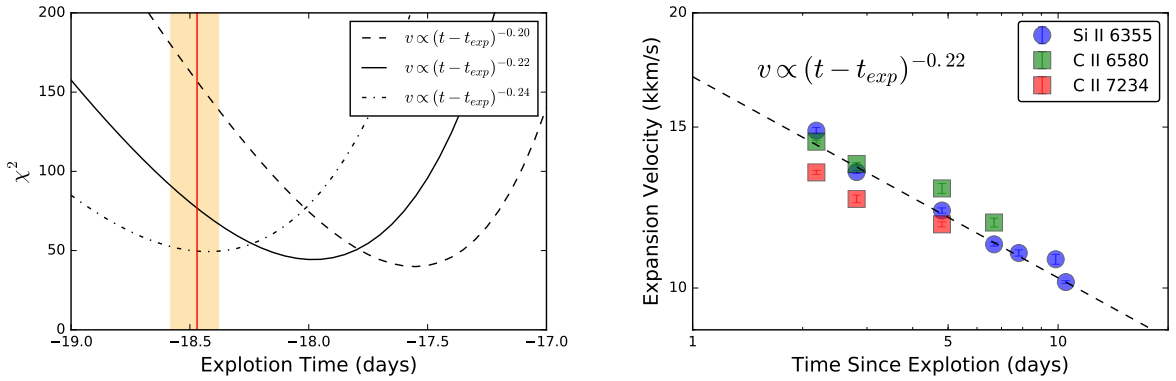

Figure 5. Constraints on t_{exp} from fitting the velocity evolution of Si II. *Left panel:* the dashed, solid and dash-dotted curves show χ^2 for fitting power laws with indices -0.20, -0.22 and -0.24, respectively. The red vertical line and the orange region indicate t_0 and its 3-σ confidence interval from Section 4.1. *Right panel:* Observed Si II 6355 velocities and the best-fit power-law velocity with an index of -0.22.

C II features are not strong in the first spectra (Parrent et al. 2012). The only normal SN Ia known to have strong C II features at early phases is SN2013dy (Zheng et al. 2013). Unlike iPTF16abc, however, the equivalent

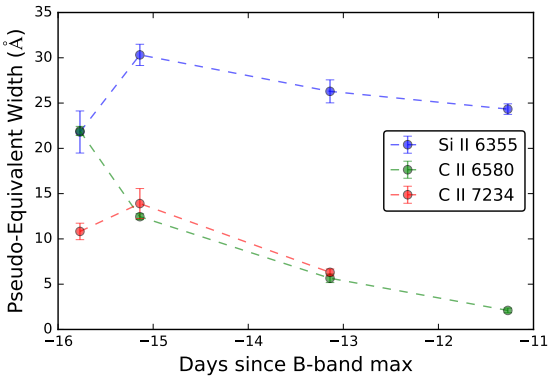

Figure 6. Pseudo-equivalent width of Si II 6355, C II 6580 and C II 7234 lines. The uncertainties in these measurements are less than the sizes of these symbols.

widths of C II features in SN2013dy are as large as those of Si II 6355 in the same spectra.

4.4. *Discussions*

Early radiation of a SN Ia may have multiple energy sources: SN shock breakout, SN-companion collision, and radioactive activity. The previous analysis is based on the assumption that the light curve of iPTF16abc is powered purely by radioactive decay. Here we discuss the other two possibilities.

4.4.1. *SN Shock Breakout*

The shock breakout of a SN Ia lasts for a fraction of a second due to the small size of the exploding star. However, the subsequent cooling phase may last longer (e.g., Piro et al. 2010). Following the analysis of SN2011fe in Bloom et al. (2012), we compare the early-phase g-band light curve of iPTF16abc with two cooling models (Rabinak & Waxman 2011; Piro et al. 2010) and reach a not very constraining conclusion that the radius of the progenitor star of iPTF16abc should be $< 1R_{\odot}$. In fact, with a typical $0.01R_{\odot}$ radius of a white dwarf, the cooling emission of a SN Ia is negligible at the time of the first detection of iPTF16abc.

4.4.2. *SN-Companion collision*

From a SN Ia born in a single-degenerate system, with an odd of $\lesssim 10\%$ due to the geometry, we expect to see emission produced by SN ejecta slamming into the companion. According to calculations by Kasen (2010), collision between SN ejecta and the companion star generates thermal emission with a spectrum with spectrum that peaks in the ultraviolet. The Rayleigh-Jeans tail emission in the g band is very weak.

In order to examine the possible SN-companion signature in the early light curve of iPTF16abc, we employ the Kasen (2010) model by assuming an ejecta mass of $1.4M_{\odot}$, an expansion velocity of $10^4\,\mathrm{km\,s^{-1}}$, and a constant opacity of $0.2\,\mathrm{cm^2\,g^{-1}}$. The angular dependence of this emission uses the parameterized equation in Brown et al. (2012). Figure 7 compares the calculated g-band apparent magnitudes of SN-companion collision for different combinations of binary separation and viewing angle against the first detection of iPTF16abc. The figure shows that, even with the most favored viewing angle, the binary separation would have to exceed 2×10^{14} cm. Under the model assumption that the companion fills its Roche lobe, the companion star would have to have a radius of $\sim 10^{14}\,\mathrm{cm} \simeq 10^4 R_{\odot}$. Given that the mass of the companion is $\sim 1R_{\odot}$, such a large radius seems unlikely. Therefore, we conclude that the early emission of iPTF16abc is not likely to originate from the SN-companion collision.

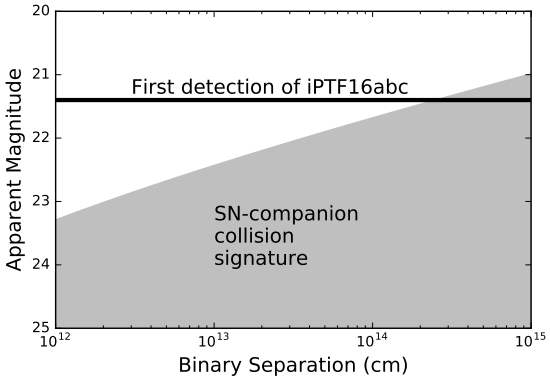

Figure 7. apparent magnitude of SN-companion collision (gray region) against the first detection of iPTF16abc (black).

5. CONCLUSION

In this paper, we present observations of an extraordinarily young normal Type Ia supernova iPTF16abc at one tidal tail of NGC 5221. Our extraordinarily fast-response follow-up compaign of this supernova allows us to draw the following conclusions:

- By extrapolating the early light curve, we determine that the first light of the SN light curve was only 0.18 days before our first observation.
- Our analysis shows that the observed early-phase light curve is probably powered by radioactive decay of ^{56}Ni, instead of SN shock breakout or SN-companion collision (provided that iPTF16abc is born in a single-degenerate channel).
- Our measurements on the spectral line velocities shows that the actual explosion date of the SN is

approximately equal to the time of the first light of the SN light curve, indicating that synthesized ^{56}Ni atoms are mixed out into the outer layers of the supernova ejecta.

- The strong mixing of ^{56}Ni is also supported by strong and short-lived carbon features in the earliest spectra of iPTF16abc.

Observations of extraordinarily young supernovae provide a "smoking gun" to probe the mixing level in the ejecta, which, in turn, results directly from the explosion mechanisms. With the ongoing and planned time-domain survyes, a large number of extraordinarily young supernovae will be collected in the next few years. With such a sample, we will be able to make connections between the observed supernovae and proposed mechanisms.

It should also be emphasized that much of the analysis presented in this paper would not be possible without the fast-response and extensive photometric and spectroscopic follow-up compaign. With the great potential of discoveries in the surveys, researchers need to be prepared and organized for follow-up observations.

YC thanks supports from the postdoc fellowship in the eScience institute, University of Washington.

REFERENCES

Adelman-McCarthy, J. K., Agüeros, M. A., Allam, S. S., et al. 2008, ApJS, 175, 297

Arnett, W. D. 1982, ApJ, 253, 785

Betoule, M., Kessler, R., Guy, J., et al. 2014, A&A, 568, A22

Bianco, F. B., Howell, D. A., Sullivan, M., et al. 2011, ApJ, 741, 20

Bida, T. A., Dunham, E. W., Massey, P., & Roe, H. G. 2014, in Proc. SPIE, Vol. 9147, Ground-based and Airborne Instrumentation for Astronomy V, 91472N

Blondin, S., & Tonry, J. L. 2007, ApJ, 666, 1024

Bloom, J. S., Kasen, D., Shen, K. J., et al. 2012, ApJL, 744, L17

Breeveld, A. A., Landsman, W., Holland, S. T., et al. 2011, in American Institute of Physics Conference Series, Vol. 1358, American Institute of Physics Conference Series, ed. J. E. McEnery, J. L. Racusin, & N. Gehrels, 373–376

Brown, P. J., Dawson, K. S., Harris, D. W., et al. 2012, ApJ, 749, 18

Cao, Y., Nugent, P. E., & Kasliwal, M. M. 2016, PASP, 128, 114502

Cenko, S. B., Cao, Y., Kasliwal, M., et al. 2016, The Astronomer's Telegram, 8909

Dekker, H., D'Odorico, S., Kaufer, A., Delabre, B., & Kotzlowski, H. 2000, in Proc. SPIE, Vol. 4008, Optical and IR Telescope Instrumentation and Detectors, ed. M. Iye & A. F. Moorwood, 534–545

Faber, S. M., Phillips, A. C., Kibrick, R. I., et al. 2003, in Proc. SPIE, Vol. 4841, Instrument Design and Performance for Optical/Infrared Ground-based Telescopes, ed. M. Iye & A. F. M. Moorwood, 1657–1669

Fitzpatrick, E. L. 1999, PASP, 111, 63

Foley, R. J., Challis, P. J., Filippenko, A. V., et al. 2012, ApJ, 744, 38

Fremling, C., Sollerman, J., Taddia, F., et al. 2016, A&A, 593, A68

Goobar, A., Kromer, M., Siverd, R., et al. 2015, ApJ, 799, 106

Guy, J., Astier, P., Baumont, S., et al. 2007, A&A, 466, 11

Hayden, B. T., Garnavich, P. M., Kasen, D., et al. 2010, ApJ, 722, 1691

Hook, I. M., Jørgensen, I., Allington-Smith, J. R., et al. 2004, PASP, 116, 425

Im, M., Choi, C., Yoon, S.-C., et al. 2015, ApJS, 221, 22

Kasen, D. 2010, ApJ, 708, 1025

Maoz, D., Mannucci, F., & Nelemans, G. 2014, ARA&A, 52, 107

Miller, A. A., Laher, R., Masci, F., et al. 2016, The Astronomer's Telegram, 8907

Ofek, E. O., Laher, R., Surace, J., et al. 2012, PASP, 124, 854

Oke, J. B., Cohen, J. G., Carr, M., et al. 1995, PASP, 107, 375

Olling, R. P., Mushotzky, R., Shaya, E. J., et al. 2015, Nature, 521, 332

Parrent, J. T., Thomas, R. C., Fesen, R. A., et al. 2011, ApJ, 732, 30

Parrent, J. T., Howell, D. A., Friesen, B., et al. 2012, ApJL, 752, L26

Pereira, R., Thomas, R. C., Aldering, G., et al. 2013, A&A, 554, A27

Phillips, M. M. 1993, ApJL, 413, L105

Phillips, M. M., Simon, J. D., Morrell, N., et al. 2013, ApJ, 779, 38

Piro, A. L., Chang, P., & Weinberg, N. N. 2010, ApJ, 708, 598

Piro, A. L., & Morozova, V. S. 2016, ApJ, 826, 96

Piro, A. L., & Nakar, E. 2014, ApJ, 784, 85

Poznanski, D., Prochaska, J. X., & Bloom, J. S. 2012, MNRAS, 426, 1465

Rabinak, I., & Waxman, E. 2011, ApJ, 728, 63

Schlafly, E. F., & Finkbeiner, D. P. 2011, ApJ, 737, 103

Shappee, B. J., Piro, A. L., Holoien, T. W.-S., et al. 2016, ApJ, 826, 144

Silverman, J. M., & Filippenko, A. V. 2012, MNRAS, 425, 1917

Starr, B. M., Luppino, G. A., Cuillandre, J.-C., & Isani, S. 2000, in Proc. SPIE, Vol. 3965, Sensors and Camera Systems for Scientific, Industrial, and Digital Photography Applications, ed. M. M. Blouke, N. Sampat, G. M. Williams, & T. Yeh, 58–69

Theureau, G., Bottinelli, L., Coudreau-Durand, N., et al. 1998, A&AS, 130, 333

Theureau, G., Hanski, M. O., Coudreau, N., Hallet, N., & Martin, J.-M. 2007, A&A, 465, 71

Thomas, R. C., Aldering, G., Antilogus, P., et al. 2011, ApJ, 743, 27

Valenti, S., Howell, D. A., Stritzinger, M. D., et al. 2016, MNRAS, 459, 3939

Vernet, J., Dekker, H., D'Odorico, S., et al. 2011, A&A, 536, A105

Whelan, J., & Iben, Jr., I. 1973, ApJ, 186, 1007

Zacharias, N., Finch, C. T., Girard, T. M., et al. 2013, AJ, 145, 44

Zheng, W., & Filippenko, A. V. 2016, ArXiv e-prints, arXiv:1612.02097

Zheng, W., Kelly, P. L., & Filippenko, A. V. 2016, ArXiv e-prints, arXiv:1612.02725

Zheng, W., Silverman, J. M., Filippenko, A. V., et al. 2013, ApJL, 778, L15

Zheng, W., Shivvers, I., Filippenko, A. V., et al. 2014, ApJL, 783, L24